Simulating the bio–nanoelectronic interface

2007 J. Phys.: Condens. Matter 19 215205

(http://iopscience.iop.org/0953-8984/19/21/215205)

IOP PUBLISHING JOURNAL OF PHYSICS: CONDENSED MATTER

J. Phys.: Condens. Matter **19** (2007) 215205 (12pp) doi:10.1088/0953-8984/19/21/215205

Simulating the bio–nanoelectronic interface

Campbell Millar, Scott Roy, Andrew R Brown and Asen Asenov

Department of Electronics and Electrical Engineering, University of Glasgow, Rankine Building, Oakfield Avenue, Glasgow G12 8LT, UK

E-mail: c.millar@elec.gla.ac.uk

Received 13 October 2006, in final form 7 January 2007
Published 1 May 2007
Online at stacks.iop.org/JPhysCM/19/215205

Abstract

As the size of conventional nano-CMOS devices continues to shrink, they are beginning to approach the size of biologically relevant macromolecules such as ion channels. This, in concert with the increasing understanding of the behaviour of proteins *in vivo*, creates the potential for a revolution in the sensing, measurement and interaction with biological systems.

In this paper we will demonstrate the theoretical possibility of directly coupling a nanoscale MOSFET with a model ion channel protein. This will potentially allow a much better understanding of the behaviour of biologically relevant molecules, since the measurement of the motion of charged particles can reveal a substantial amount of information about protein structure–function relationships. We can use the MOSFET's innate sensitivity to stray charge to detect the positions of single ions and, thus, better explore the dynamics of ion conduction in channel proteins. In addition, we also demonstrate that the MOSFET can be 'tuned' to sense current flow through channel proteins, thus providing, for the first time, a direct solid state/biological interface at the atomic level.

(Some figures in this article are in colour only in the electronic version)

1. Introduction

Current predictions from the ITRS (International Road-map for Semiconductors) [1] are that commercial semiconductor devices will have reached sub-10 nm dimensions within the next 10–15 years. They will then be of a directly comparable size to a significant number of biologically important macromolecules. In fact, for the first time, the ITRS 2005 edition [1] specifically mentions biological molecules as an area of emerging technological research which will be of direct relevance to the future of the semiconductor industry. As figure 1 illustrates, the extremely small scale of future CMOS devices mean that the possibility exists for them to be directly integrated into the biological domain via charge transporters such as the class of proteins known as ion channels [2]. Figure 1 shows the KCSA bacterial potassium channel from

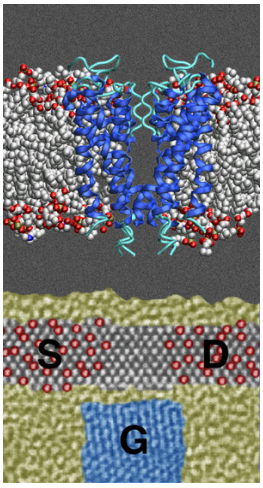

Figure 1. The bacterial ion channel Kcsa, from *Streptomyces lividans* acting as the second gate in a putative bio–nano-CMOS device, constructed from a 4 nm double-gate MOSFET with the top gate removed to expose the insulating silicon dioxide layer. Note that the relative scales of the MOSFET and biological molecule are approximately correct.

Streptomyces lividans (pdb i.d. 1K4C [3, 4]) in a position to supply gating charge to a 4 nm channel length double-gate MOSFET, which has already been demonstrated as a functional device [5, 6].

Ion channels are a class of proteins forming macromolecular pores which evolved approximately three billion years ago [2] as a method of transferring electrolytes across the cell membrane. In biological terms, the importance of this group of proteins cannot be overstated. Without a controllable method of electrolyte transfer, cells would rapidly lose or gain ions in such a way as to completely destroy the delicate balance of homeostasis required for cell survival and function. An understanding of their behaviour is also of vital importance to the medical [7] and pharmaceutical industries since a large number of drug targets are channel proteins: according to Terstappen and Reggiani [8] approximately 15% of potential drug targets are ion channels and around 45% are membrane proteins, (mostly G–protein coupled receptors). Despite the importance of these molecules, relatively little was known about their microscopic structure [9, 10] until quite recently, and little is still known about the structure–function relationships which provide the wide array of behaviours found in channel proteins. Since the primary activity of ion channels is to conduct ions during the action potential of neurons [2], it is necessary for any bio–nanodevice to be capable of sensing, not only the positions of individual ions, but the current which is passing through the channel. In doing so, we hope to be able to monitor the activity of individual ions in real time and at the atomic scale.

Currently there are many simulation studies under way which are shedding light on the properties of channel proteins [11–17]. Biological systems and semiconductors have already been interfaced on the macroscopic scale [18–20] but not in such a way as to truly integrate the biological elements of a system with semiconductors. In this paper we will not focus on the simulation of channels or the practical complexities of building such a device, but will expand upon previous work [21, 22] on the theoretical mechanisms by which a channel protein can be integrated with CMOS transistors, in such a way as to provide a multi-function, tunable, bio–nano-CMOS device.

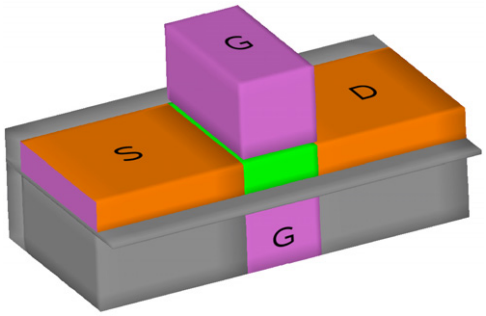

Figure 2. The double-gate MOSFET simulation structure. Source (S) and drain (D) regions are shown on the left and right of the device (in orange), gate (G) regions at the top and bottom (in purple) and the channel occupies the centre of the device (in green).

2. Simulation methodology

Our simulation study was carried out using the Synopsys Taurus simulation software [23], a commercially available drift diffusion (DD) TCAD simulator designed for the simulation and prototyping of semiconductor devices. As a general solver of the drift diffusion equations, the software allows access to many of the material and physical parameters, allowing nominally semiconducting materials to be modified to mimic the biological materials relevant in the simulation of bio–nano-CMOS devices. Since all of the simulations are performed within a unified structure the physical conditions in biological and semiconductor regions of the simulation domain are fully consistent with each other.

We have previously demonstrated that commercial TCAD software can be modified to simulate model ion channel structures which replicate the behaviour of several ion channel proteins [13]. It has been shown that the DD equations can be used to model the motion of charged ions in solutions [24], and that with appropriate calibration we can match experimental measurements of ionic currents through channel proteins.

The basis of the simulation structures used in this work is a 5 nm shallow trench isolated double-gate MOSFET whose structure is shown in figure 2. The MOSFET has a 5 nm long, 10 nm wide and 2 nm thick channel, with gate oxide thickness of 0.3 nm. The source and drain regions of the device are n-doped at a concentration of 2×10^{21} cm^{-3} and the channel is p-doped at 1×10^{16} cm^{-3}. The top and bottom gates are defined as a generic conducting material (approximating a metal) with a work function of 4.5 eV. We have chosen to simulate an idealized device, so regions are specified as simple cuboids of material surrounded by silicon dioxide. In order to emphasize the interactions between the MOSFET and the biomimetic regions of the simulation we use a constant mobility model in both the transistor and biological regions.

In order to model the biological regions in the simulations, the physical parameters of the materials in Taurus must be modified. Table 1 gives a list of the important physical parameters used in the various relevant materials. For example, silicon, as a conducting material, has been modified to behave as an analogue of an electrolyte solution with a relative dielectric constant of 80. The extremely low mobility of ions, when compared to electrons and holes, presents some novel numerical problems, when coupling electron and ion transport in a single simulation domain, and great care must be taken to ensure the correct convergence of numerical solvers for all carrier types. A layer of silicon dioxide is used to provide an insulating region similar in behaviour to the lipid membrane in cells. This region is ascribed a relative dielectric constant of 2. This value is somewhat arbitrary since all that is required of the lipid region is to

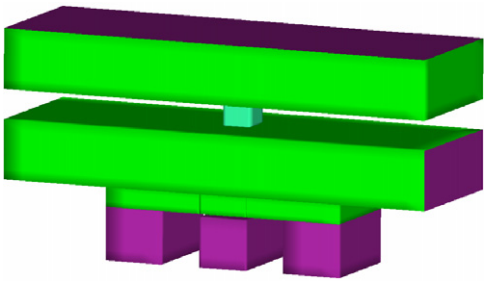

Figure 3. The bio–nano-MOSFET simulation structure. Silicon regions are shown in green (light grey); the electrode is purple (dark grey). All insulating oxide has been removed to show the internal structure of the device.

Table 1. The physical simulation parameters used for all simulations. Values for biomimetic materials are modified from the Taurus defaults. Details of other parameters are available from [25].

Taurus material	Physical material	μ_e ($m^2\ V^{-1}\ s^{-1}$)	μ_p ($m^2\ V^{-1}\ s^{-1}$)	ϵ_r
Si	Si	1.4×10^{-1}	4.5×10^{-2}	11.9
Si	H_2O	7.62×10^{-8}	7.62×10^{-8}	80
SiO_2	SiO_2	0	0	3.9
SiO_2	Phospholipid	0	0	2
Si_3N_4	Protein	0	0	20
Electrode	Conductor	NA	NA	1

act as a separator between the intracellular and extracellular environments and to ensure that a significant proportion of the membrane potential is dropped across this region. A 3 nm aperture is created in the insulating oxide layer and is filled with silicon nitride (again as an insulator) whose properties have been modified to mimic the body of the channel protein itself. The pore is then created as a silicon/electrolyte filled region through the centre of this protein. In the case of all simulations presented here the pore has a square cross section of 0.6 nm × 0.6 nm.

The final structure of the bio–nano-MOS device can be seen in figure 3, where the insulating oxide regions have been removed for clarity. The double-gate structure is modified by the removal of the top gate and all oxide above the gate insulating layer. This is replaced with ambient air to create a single-gate/double-gate device. The ambient region is then filled with two 6 nm thick layers of electrolyte/silicon separated by a 3 nm thick lipid/oxide layer. The pore region is then created over the centre of the MOSFET channel. Electrical contacts are made along the top (intracellular) surface of the top bath region as well as on either side of the bottom bath region. These act as particle sources and sinks, allowing current flow through the pore region, resulting in the final structure shown in figure 3.

We must now examine the impact that these biological modifications have on the MOSFET device performance. Figure 4 compares the I_d–V_g characteristics of three different MOSFET configurations. The first is a standard double-gate structure. The second is a single-gate structure, created by replacing everything above the oxide layer at the top of the channel with air, and the third is the full bio–nano-MOSFET structure. Figure 4 shows that there is significant degradation of the sub-threshold slope, electrostatic integrity and gating efficiency of the device when coupled to the biomimetic regions. In the sub-threshold region of operation the device sensitivity, to the gate (and other) potentials, drops from 60 mV/decade in the double-gate device to 110 mV/decade in the single gate, and finally to a very poor 250 mV/decade. However, as we will demonstrate, for our purposes this gate sensitivity is sufficient.

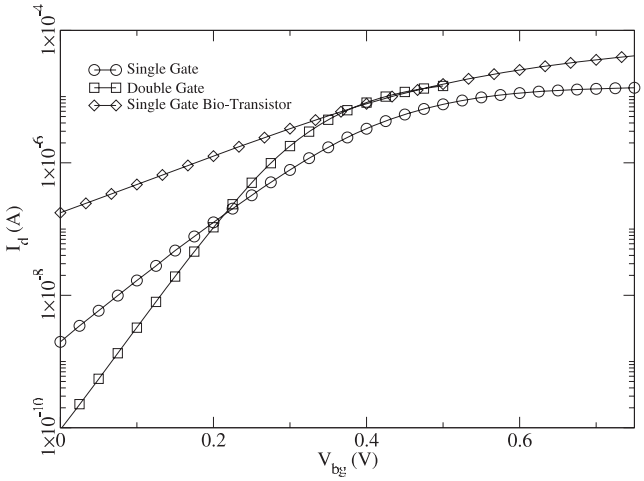

Figure 4. MOSFET I_d–V_g characteristics for the three simulation configurations.

3. Electrostatic sensitivity

The sensitivity of small MOSFETs to stray charges is well known [26]. We can exploit this, otherwise problematic, phenomenon to measure the transport of ions through ionic channels. We dope the top bath region of the simulation at 6×10^{20} cm^{-3} to mimic a 1 M salt solution, the doping in the bottom bath should be kept as low as possible in order to ensure that as much potential as possible is dropped over this region to maintain the electrostatic sensitivity of the device. In practice, it was found that doping the bottom bath below the equivalent of 1 mM (6×10^{17} cm^{-3}) was a reasonable compromise between numerical stability of the simulation and the sensitivity of the device.

The electrostatic sensitivity is measured by applying the surface charge model available in Taurus, to a small element of the correct volume. By careful control of the simulation mesh in the pore region of the domain, a mesh element of the appropriate volume and surface area can be created, resulting in a localized static charge of 1.6×10^{-19} C at the desired position. This charge can then be moved down the pore toward the MOSFET surface, in order to simulate the motion of a potassium ion across the membrane. The MOSFET is biased with 100 mV applied to the drain and held in the sub-threshold region of operation with a gate voltage of 200 mV.

The response of the MOSFET to a single charge can be seen in figure 5. As the charge is moved down the length of the pore a drain current change of $\sim$57 nA nm^{-1} is observed, indicating the electrostatic sensitivity of this device. Note that the non-linearity in response at the upper end of the pore indicates that this device is most effective at low ionic concentrations, where screening from other mobile charges is minimized. It should be noted that in any real system there will be additional electrical and ionic thermal noise. As figure 5 shows, not only is the device capable of detecting charges inside the pore, but also of resolving their position. Therefore, such bio–nanodevices could potentially be utilized, not only as an interface between solid state and biological systems, but also as a method of probing the mechanisms whereby complex biological molecules (such as ion channels) perform their myriad functions.

4. Current sensitivity

One of the goals of the integrating biological and solid state devices is to directly interface solid state circuits with biological systems which may be utilized as: direct neural interfaces,

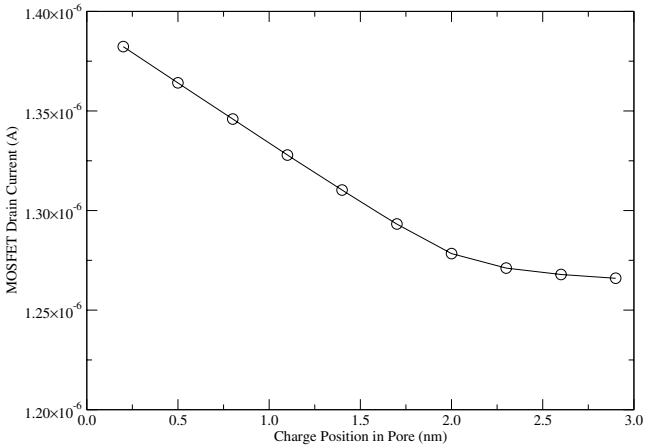

Figure 5. MOSFET electrostatic sensitivity. The MOSFET source–drain current is measured for various positions of a test charge within the 3 nm long pore region. 0 nm corresponds to the bottom of the lipid/oxide layer which is 6 nm from the MOSFET gate dielectric. Note that the non-linear response at the upper end of the pore is due to heavy doping in the top bath screening the test charge.

biological computing elements or as very sensitive single-molecule biosensors. In order to achieve this we need to demonstrate that a MOSFET can be used to measure the activity of an ion channel.

In the previous examples, all contact regions in the device have simply been set to 0 V as simple boundary conditions for the solution of the Poisson equation, apart from the bottom bath particle sinks which are allowed to float. However, in order to measure the effect of pore current on the MOSFET we now require that a potential difference be created across the lipid membrane and that the current continuity equations are solved in the biological region of the simulation. This greatly affects the numerical stability of the solution as we now have charge carriers moving with very different mobilities in close proximity to one another.

If one applies a potential to the top bath contact and treats the bottom bath contact regions as a 0 V reference, then one would expect current to flow through the pore in an approximately Ohmic fashion [27]. However, this is not the case. There is a substantial difference in carrier energy (shown in figure 6) between the heavily n-doped semiconductor and the p-doped bath region, causing significant depletion in the bottom bath. This results in a significant drop in the conductivity of the bottom bath and a corresponding non-linear drop in the pore current to close to zero.

To ensure that the pore current *can* be measured we adjust for this offset in the energy levels between the biological and semiconductor regions of the device, by applying an offset potential (V_{off}) which compensates for the corresponding built in potentials and aligns the valence and conduction bands in the two regions. The applied offset potential which is required to align the bands is known as the flat band potential (V_{fb}). Since we have p-doped silicon in the bottom bath and heavily n-doped source and drain regions the built in potential, in this case, is approximately the band-gap of silicon (1.12 eV), the difference between the valence and conduction bands. Obviously, in a real system with an electrolyte solution this value will be different. The value of the flat band potential (V_{fb}) is not known *a priori*, but can be determined experimentally from C–V measurements of the combined MOS–electrolyte device [28] or estimated theoretically [29], and will be close to the difference in work function (ϕ) between the semiconductor and the electrolyte ($V_{\text{fb}} = \phi_{\text{electrolyte}} - \phi_{\text{Si}}$). However, as we will see later the absolute value of V_{fb}

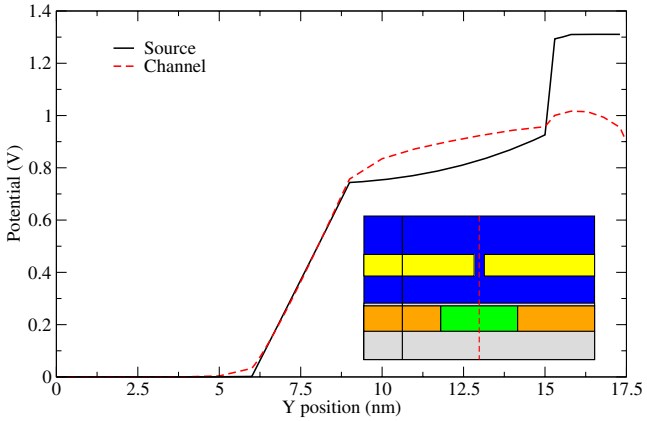

Figure 6. The potential profile plotted vertically through the simulation structure with all contact regions set to 0 V. The inset shows the regions through which the data have been extracted.

Figure 7. The potential profile through the centre of the simulation domain. (a) shows the result of a poor choice of offset potential where $V_{\text{off}} = 0.5$ V. The bottom bath region is strongly affected by the conditions in the MOSFET. (b) shows the flat band condition, when $V_{\text{off}} = V_{\text{fb}}$, where the potential distribution through the biological portion of the domain is more uniform.

is of little practical importance since V_{off} is a parameter which can be used to tune the physical response of the device to an operating point where the desired behaviour is obtained.

The full effect of the choice the applied offset potential (V_{off}) can be seen in figures 7 and 8 which show the potential and hole concentration profiles at $V_{\text{off}} = V_{\text{fb}} = 1.1$ V and where $V_{\text{off}} = 0.5$ V which illustrates a condition far away from the ideal flat band condition and in practice was the minimum potential where the simulations remained numerically stable, since below this point the pore current becomes extremely small. As can be seen in figures 7, 8 and 9 there is significant potential drop and depletion in the bottom bath at $V_{\text{off}} = 0.5$ V. At $V_{\text{off}} = V_{\text{fb}}$, however, there is little change in the bottom bath hole concentration and the potential drop is minimal. The slight variation which can be seen along the length of the device is due to the difference in the energy offset between the heavily n-doped source and drain regions and the lightly p-doped channel region, as shown in figure 6.

We must now demonstrate that the pore replicates reasonably the range of behaviour that we would expect from a channel protein. Ionic currents through ion channels typically have magnitudes in the 10–100 pA range [2, 30], with a quite complex range of I–V characteristics. Our simple pore will not reproduce the more complex channel behaviour, such as rectification,

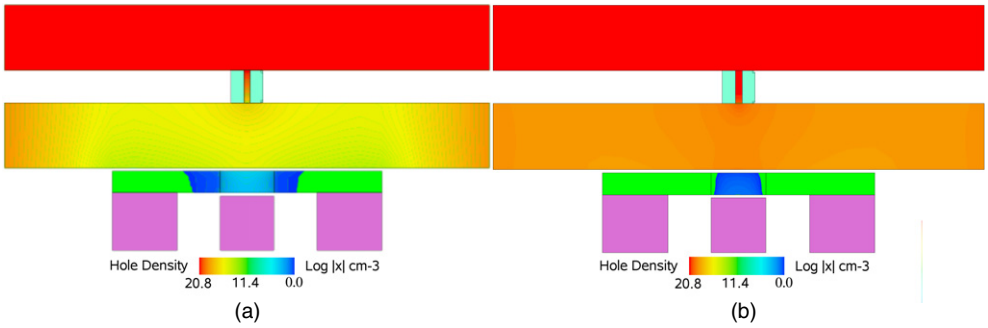

Figure 8. Hole concentration profiles through the centre of the simulation domain for $V_{\text{off}} = 0.5$ V (a) and $V_{\text{off}} = V_{\text{fb}}$ (b). Note the depletion of the bottom bath at $V_{\text{off}} = 0.5$ V and that, at the flat band potential, there is little effect on the bottom bath hole concentration.

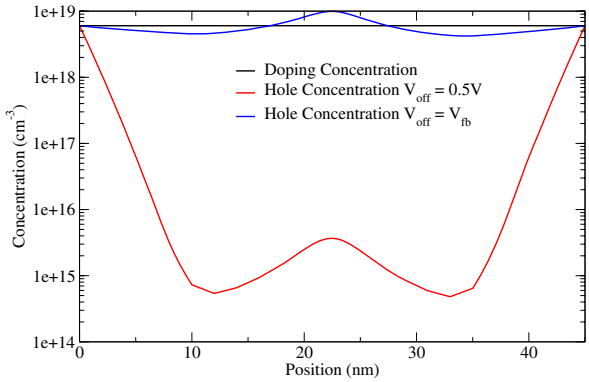

Figure 9. Hole concentration extracted across the centre of the bottom bath for V_{off} equals 0.5 V and V_{fb}. The effect of the heavily n-doped source and drain regions can be clearly seen.

nor would we expect it to. For our purposes, it is simply enough to quantitatively reproduce the range of channel currents. In all cases that follow the simulation configuration is as follows: top bath doping, 6.02×10^{20} cm^{-3}, bottom bath doping, 6.02×10^{18} cm^{-3}, bottom bath contact regions set as the 0 V reference, source voltage $= V_{\text{off}}$, drain voltage $= V_{\text{off}} + 0.1$ V, gate voltage $= V_{\text{off}} + 0.3$ V and the top bath contact region is set to the applied membrane potential.

Figure 10 shows the pore current as a function of the top gate potential for various values of V_{off}. As we have previously demonstrated, away from the flat band conditions the current becomes extremely small <1 pA due to the depletion of the bottom bath. However, when V_{off} is close to V_{fb} the behaviour of the model pore is approximately consistent with experimentally measured values of pore currents, i.e. of the order of pA [2, 30].

In order to demonstrate conclusively that we have created a device capable of detecting current flow through the pore, we must prove that any change in the MOSFET source drain current is due to the pore current and not some other mechanism, such as electrostatic control from the top contact potential. In order to do this we generated two simulation domains which are identical except for the inclusion of the pore. Since there can be no current flow between the top and bottom bath regions without the conduit of the pore, we can conclusively demonstrate that the MOSFET is responding to the pore current by showing that there is no change in source–drain current when the pore is not present. The results of these two simulations

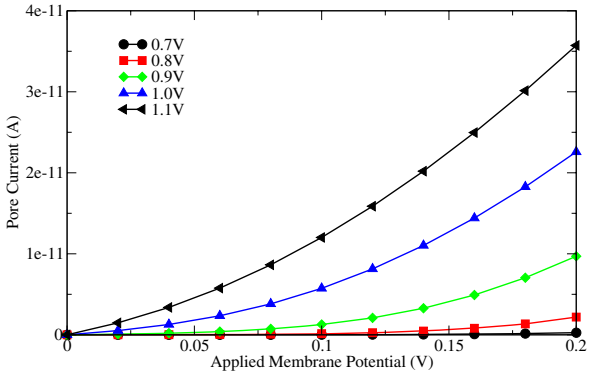

Figure 10. The pore versus top contact applied potential for various values of V_{off}. Note that below 0.7 V the current becomes practically 0.

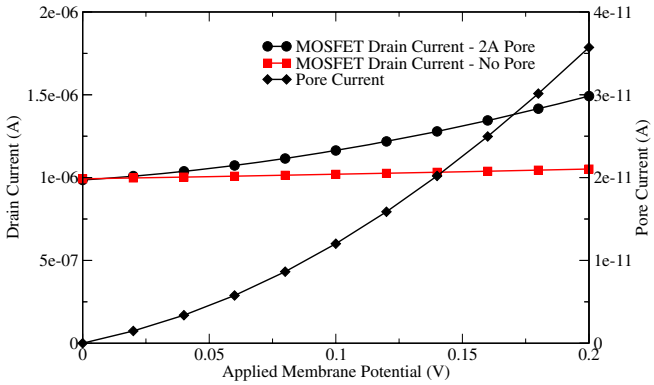

Figure 11. A comparison of the changes in MOSFET drain current with the applied membrane potential in the situation where the pore region of the simulation in present and not present. Note that with no pore the change in drain current due to the applied membrane potential is very small.

are shown in figure 11. The simulation containing a pore clearly produces a change in the drain current of approximately 50%, whereas the simulation with no pore produces a very small change in the MOSFET current, attributed to electrostatic control from the top contact. The comparison of these two results represents incontrovertible proof that the MOSFET is responding to the current flow through the pore.

Having shown that the MOSFET can respond to the ionic current we can now analyse the sensitivity of the bio–nano-MOSFET. Figure 12 shows a plot of the sensitivity of the MOSFET to the pore current, defined as

$$S = \frac{\Delta I_{\text{d}}}{\Delta I_{\text{p}}}. \tag{1}$$

It is clear that the sensitivity of the combined device strongly depends on the choice of offset potential. At $V_{\text{off}} = V_{\text{fb}}$ the response is approximately linear with a gain of $\sim$15 000, whereas at $V_{\text{off}} = 0.7$ V the sensitivity of the MOSFET to the pore current is greatly increased (by three orders of magnitude) but the linearity is significantly degraded.

Figure 13 clearly shows the linearity of the MOSFET response to the pore current. The fact that the percentage change in the drain current is linear with pore current means that, by

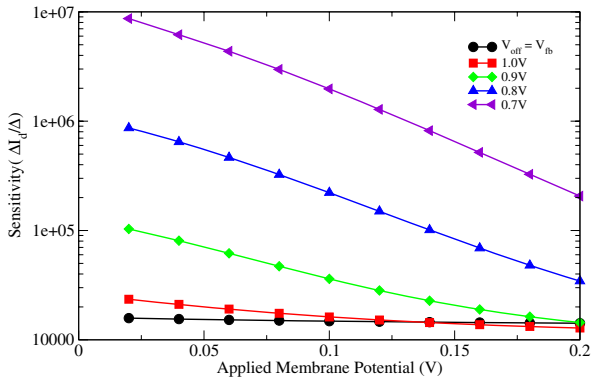

Figure 12. The MOSFET current sensitivity ($\frac{\Delta I_d}{\Delta I_p}$) measured as a function of the applied membrane potential. Note that at $V_{off} = V_{fb}$ the response is almost linear and that V_{off} significantly affects both the sensitivity and linearity of the sensor.

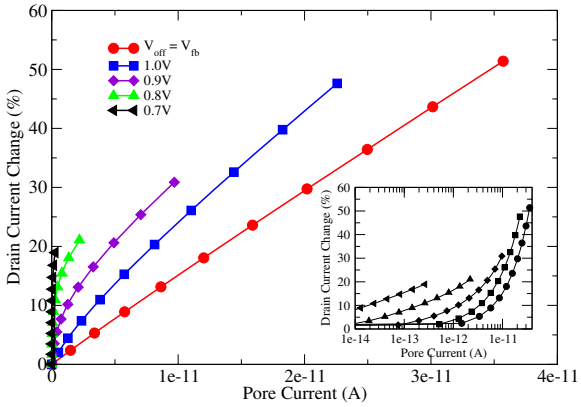

Figure 13. The response of the bio–nano-MOS device. Note the linearity of response at the flat band condition and the extreme sensitivity of the device away from this operating point. The inset shows more clearly just how electrostatically sensitive the response becomes away from V_{fb}.

adjusting the biasing conditions of the MOSFET, we can increase or decrease the gain of the sensor. For example, a gate bias of 0.4 V will produce an increase in the drain current of ∼25% when compared to a bias of 0.3 V.

$$\Delta I_d(V) = 100 \times \frac{(I_V - I_0)}{I_0}. \tag{2}$$

This is clearly demonstrated in figure 13 where the percentage change in the drain current (defined in equation (2)) shows excellent linearity of response. This indicates that we can also adjust the gain of the device at the flat band condition, by changing the biasing of the MOSFET, without affecting the response to the pore current. We can also see that V_{off} can be used as a 'tuning' parameter which allows the operation of the device to be changed. As figures 12 and 13 show, if V_{off} is chosen so that depletion of the bottom bath occurs, the electrostatic sensitivity of the device is increased. This indicates that by choosing the relevant value of V_{off} the bio–nano-MOSFET can be optimized, either as a current sensor/amplifier or a single-charge sensor. Obviously the choice of V_{off} in reality will be governed by the specific mode of operation required from the sensor as well as external factors such as noise thresholds etc. However, in

general, the ability to tune the operating point of a bio–nanosensing device is likely to be of great use.

5. Conclusions

With the scaling of CMOS technology the direct interaction between biological systems and solid state can become a reality. In this paper, we have demonstrated that it is, at the very least, theoretically possible to directly couple a suitably modified nanoscale MOSFET transistor and biologically significant macromolecules. We have demonstrated that this integrated device can be used to sense the individual ions passing through channel proteins *in vitro* as well as to measure the current flow across cell membranes. All of this raises the following possible applications:

(i) The bio–nanodevice can be used to measure the conductance of single-ionic channels, potentially replacing the use of patch clamp measurements.
(ii) The utilization of the device as a single-atom biosensor for detecting e.g. channel blocking heavy metals.
(iii) It may allow us to monitor ion channel dynamics *in vivo*, and as never before, in real time.
(iv) An array of such devices could be utilized, along with an appropriate addressing mechanism, to measure the distribution and function of ion channels over the cell membrane.

The above will allow us to significantly increase our knowledge about the mechanisms governing ion channel conduction. Also, for the first time this raises the realistic possibility of electron/ion computing which may lead to the exploitation of biological computing elements and/or the direct integration of solid state devices as elements or monitors of active biological processes.

References

[1] ITRS 2005 http://www.itrs.net/Links/2005ITRS/Home2005.htm
[2] Hille B 2001 *Ion Channels of Excitable Membranes* (Sunderland: Sinauer)
[3] Zhou Y, Morais-Cabral J H, Kaufman A and MacKinnon R 2001 *Nature* **414** 43–8
[4] The Protein Data Bank http://www.rcsb.org/pdb/index.html
[5] Wakabayashi H, Yamagami S, Ikezawa N, Ogura A, Narihiro M, Arai K, Ochiai Y, Takeuchi K, Yamamoto T and Mogami T 2003 *IEDM '03 Technical Digest* IEEE International
[6] Wakabayashi H, Ezaki T, Sakamoto T, Kawaura H, Ikarashi N, Ikezawa N, Narihiro M, Ochiai Y, Ikezawa T, Takeuchi K, Yamamoto T, Hane M and Mogami T 2006 *IEEE Trans. Electron Devices* **53** 1961–70
[7] Ashcroft F 2000 *Ion Channels and Disease* (San Diego, CA: Academic)
[8] Terstappen G C and Reggiani A 2001 *Trends Pharmacol. Sci.* **22** 23–6
[9] Doyle D A, Cabral J M, Pfuetzner R A, Kuo A, Gulbis J M, Cohen S L, Chait B T and MacKinnon R 1998 *Science* **280** 69–77
[10] Jiang Y, Lee A, Chen J, Cadene M, Chait B and Mackinnon R 2002 *Nature* **417** 523–6
[11] Tielman D, Biggin P, Smith G and Sansom M 2001 *Q. Rev. Biophys.* **34** 473–561
[12] Im W and Roux B 2002 *J. Mol. Biol.* **322** 851–69
[13] Millar C 2004 3D simulation techniques for biological ion channels *PhD Thesis* University of Glasgow, Glasgow
[14] Roux B and Schulten K 2004 *Structure* **12** 1343–51
[15] Millar C and Asenov A 2005 *Handbook of Theoretical and Computational Nanotechnology* (Stevenson Ranch, CA: American Scientific Publishers) chapter (P3M Simulation of Biological Ion Channels)
[16] Roux B 2005 *Annu. Rev. Biophys. Biomol. Struct.* **34** 153–71
[17] Beckstein O and Sansom M S P 2006 *Phys. Biol.* **3** 147–59 (http://stacks.iop.org/1478-3975/3/147)
[18] Fromherz P 2002 *ChemPhysChem* **3** 276–84
[19] Fromherz P 2001 *Technical Digest of the International Electronics Devices Meeting* (San Francisco, CA: IEEE)

[20] Völker M and Fromherz P 2005 *Small* **1** 206–10
[21] Millar C, Asenov A, Brown A and Roy S 2005 *IEEE Transactions on Nano-Technology, IEEE-NANO 05* (Piscataway, NJ: IEEE) pp 325–8 (IEEE Transactions) invited Paper
[22] Millar C, Asenov A and Roy S 2006 *E-MRS IUMRS ICEM (Strasbourg: 2006) Spring Meeting, Symposium Q* EMRS
[23] 2004 *Medici-Taurus, Process and Device Simulator* http://www.synopsys.com
[24] Hess K, Ravaioli U, Aluru N, Gupta M and Eisenberg R 2001 *VLSI Des.* **13** 179
[25] *Synopsis Taurus Process and Device Manual* http://www.synopsis.com
[26] Asenov A, Brown A, Davies J, Kaya S and Slavcheva G 2003 *IEEE Trans. Electron Devices* **50** 1837–52
[27] Millar C, Roy S, Beckstein O, Sansom M and Asenov A 2007 *J. Comp. Elec.* Online at http://www.springerlink.com/content/t4rv583207778167/
[28] Jakobson C G, Sudakov-Boreysha L, Fiensod M, Dinar U and Nemirovsky Y 2000 *Proc. 21st IEEE Convention of the Electrical and Electronic Engineers in Israel* (Piscataway, NJ: IEEE) pp 61–4 (ieeexplore.ieee.org)
[29] Siu W M and Cobbold R S 1979 *IEEE Trans. Electron Devices* **26** 1805–15
[30] LeMasurier M, Heigenbotham L and Miller C 2001 *J. Gen. Physiol.* **118** 303–13